Journal of Solid State Chemistry 184 (2011) 351–356

Contents lists available at ScienceDirect

Journal of Solid State Chemistry

journal homepage: www.elsevier.com/locate/jssc

# Unexpected formation by pulsed laser deposition of nanostructured Fe/olivine thin films on MgO substrates

C. Legrand [a], L. Dupont [a], C. Davoisne [a], F. Le Marrec [b], J. Perrière [c], E. Baudrin [a,*]

[a] Laboratoire de Réactivité et Chimie des Solides, UMR CNRS 6007, Université de Picardie Jules Verne, 33, rue Saint Leu, 80039 Amiens CEDEX, France
[b] Laboratoire de Physique de la Matière Condensée, UFR des Sciences, Université de Picardie Jules Verne, 33, rue Saint Leu, 80039 Amiens CEDEX, France
[c] Institut des NanoSciences de Paris, UMR CNRS 7588, Université Paris 6, 140 rue de Lourmel, 75015 Paris, France

ARTICLE INFO

*Article history:*
Received 21 July 2010
Received in revised form
19 November 2010
Accepted 23 November 2010
Available online 1 December 2010

*Keywords:*
Thin films
Pulsed laser deposition
Nanostructure
Olivine

ABSTRACT

Olivine-type $LiFePO_4$ thin films were grown on MgO (1 0 0) substrates by pulsed laser deposition (PLD). The formation of an original nanostructure is evidenced by transmission electron microscopy measurements. Indeed, on focused ion beam prepared cross sections of the thin film, we observe, the amazing formation of metallic iron/olivine nanostructures. The appearance of such a structure is explained owing to a topotactic relation between the two phases as well as a strong Mg diffusion from the substrate to the film surface. Magnesium migration is thus concomitant with the creation of metallic iron domains that grow from the core of the film to the surface leading to large protuberances. To the best of our knowledge, this is the first report on iron extrusion from the olivine-type $LiFePO_4$.



## 1. Introduction

With the objective to improve the energy storage of lithium-ion cells, numerous studies were performed on various electrode materials during the last 30 years. With the decrease of the fossil energy stocks, the development of such cell is becoming a strategic problem, namely to be able to switch towards a cleaner transportation with electric or hybrid vehicles. While lots of improvements have been obtained through cell design and optimization, there is still a material challenge to improve the storage capacities leading to higher gravimetric and volumetric energy densities. Besides the applied studies aiming to increasing materials performance, there are also lots of fundamental questions on the structural and physical properties of such specific class of materials. Of peculiar importance is the role of transport properties on materials performances and its optimization through electrode design [1]. To understand the origin of ionic and/or electronic limitations which frequently reduce the performance of materials, thin film studies can bring new important insights with the possibility to control either the thickness or the texturation of the films [2–6].

The $LiMPO_4$ orthophosphate family (with $M$=Mn, Fe, Co and Ni) became the focus of numerous studies since the first demonstration of the good electrochemical activity of $LiFePO_4$ as cathode material (with a capacity of 170 mAh/g at 3.42 V vs. $Li^+/Li^0$) [7,8]. This latter material, which presents cost and environmental impact advantages [9–12], shows however low electronic and ionic conductivity at room temperature ($\approx 10^{-9}$ to $10^{-10}$ S cm$^{-1}$) [13–15] and thus necessitates either to reduce the particles size (to reduce the diffusion length of lithium) [8,16] or to use carbon coating tricks [17,18] to obtain the expected full theoretical capacity [5,19]. Furthermore, Morgan et al. [20] and Islam et al. [21], using an *ab initio* method or a semi-empirical model, respectively, showed that the activation energy was very low along the direction [0 1 0] and that consequently the conduction of the lithium ions would be highly anisotropic and facilitated along this direction. This was later corroborated by the model derived for the lithium extraction from hexagonal particles of $LiFePO_4$ [22].

There has thus been an interest for the formation of "model" thin films which could be orientated along that [0 1 0] direction for further characterization of the transport and electrochemical properties. Several groups tried to obtain such textured $LiFePO_4$ thin films using various deposition techniques and substrate natures [3,23–25]. Pulsed laser deposition (PLD) is particularly a rich technique owing to the different deposition parameters to tailor such films [26–28]. In previous studies, we reported on the preferential growth along the [1 2 0] direction (using the *Pmnb* space group) on silicon wafers [3]. From a fundamental point of view, PLD thin films can thus present unique microstructures or textures that, once understood, could throw new insight on materials that we have believed well known.

In this paper, we report on "olivine-type" thin films grown by PLD on (1 0 0) MgO substrates. The MgO substrate selection was based on crystallographic consideration, to force the thin film growth along the peculiar [0 1 0] direction. Although this goal was not reached, we provide here not only information on the effect of

* Corresponding author. Present address: Faculté de Pharmacie, Laboratoire des Glucides, CNRS UMR 6219, Université de Picardie Jules Verne, 1 rue des Louvels, 80037 Amiens Cedex France. Fax: +33 322827590.
*E-mail address:* emmanuel.baudrin@u-picardie.fr (E. Baudrin).

0022-4596/$ - see front matter © 2010 Elsevier Inc. All rights reserved.
doi:10.1016/j.jssc.2010.11.022

the synthesis conditions on the formed films (particularly the effect of the laser energy on the sample microstructure) but also a fine characterization of the films formed in such conditions. A comprehensive transmission electron microscopy (TEM) study was realized to determine at the nanometer scale the structure and the composition of the different domains of the films and to understand the origin of such a nanostructure. We thus demonstrate for the first time the extrusion of iron from $LiFePO_4$ in these specific conditions.

## 2. Experiment

Pure $LiFePO_4$ powder was prepared using a solution route as previously described [29]. Typically, $LiH_2PO_4$ and $Fe(NO_3)_3 \cdot 9H_2O$ aqueous solutions were mixed in stoichiometric proportions under constant stirring. First, the solvent was evaporated until the obtaining of thick beige slurry, which was subsequently dried at 300 °C under Ar flow. Then an annealing treatment was performed at 500 °C under 90:10 volume ratio $N_2/H_2$ atmosphere for 20 h using a 2 °C/min heating rate. $LiFePO_4$ powder was initially shaped as a pellet using mono-axial pressing at about 500 kg/cm$^2$ and secondly densified under isostatic conditions at about 2500 bar for 30 min. The so-obtained pellet was further sintered at 800 °C during 24 h under Ar gas flow leading to a 75% compactness target used for the PLD process.

The thin films were grown by PLD using KrF laser ($\lambda = 248$ nm). For all experiments described in this work, the Argon pressure inside the chamber was set to $8 \times 10^{-2}$ mbar, the target/substrate distance was fixed to 3 cm and a laser pulse repetition rate of 2 Hz was used, according to our previous report [27]. "$LiFePO_4$" thin films were deposited on (1 0 0) MgO single crystal (Crystal GmbH) $5 \times 5$ mm$^2$ size and 0.5 mm thick. The substrate temperature was fixed to 600 °C. Our main goal was indeed to synthesize thin films of $LiFePO_4$ with a preferential orientation according to the [0 1 0] direction. The (1 0 0) MgO substrates were thus selected because of a good appropriateness of the in plane cell parameters with the $a$ cell parameter of $LiFePO_4$ cell, as described in the results part below.

X-ray diffraction patterns were collected in a $\theta/2\theta$ Bragg–Brentano geometry using a D5000 diffractometer (with Cu $K\alpha$ radiation, $\lambda = 1.54056$ Å) operating at 40 kV and 40 mA with a scanning step of 0.02° during 15 s and a detector slit of 0.6 mm was used. The samples surfaces morphologies were determined using scanning electron microscopy (FEI Quanta 200 F). Information on the nanostructure and composition of the thin films were determined using a scanning transmission electron microscope (STEM-FEI TECNAI F20 S-TWIN) fitted with both EDAX energy dispersive spectrometer (EDS) and high angle annular dark field (HAADF) detector. Rutherford backscattering spectroscopy (RBS) with the 2.5 MeV Van de Graaff accelerator of the INSP was also used to study the film composition, as previously reported for other Li-based oxides [30]. The cross section was realized by focused ion beam (FIB) technique at Institut d'Electronique, de Microélectronique et de Nanotechnologie (IEMN) of Lille (France).

## 3. Results and discussion

### 3.1. Characterization

Using the PLD parameters detailed above, we first investigated the effect of the laser energy on the film formation. On (1 0 0) MgO substrate, whatever the laser energy, namely 90, 150 and 180 mJ, the films XRD patterns present a main peak at about 42.1° $2\theta$ suggesting a preferred orientation (Fig. 1). The portion between 42.7° and 43.7° corresponding to (2 0 0) MgO substrate is voluntarily masked for clarity reasons. Furthermore, the XRD patterns clearly underline an increase in crystallinity as the laser energy is increased. In all cases, for our measurement conditions, the rocking curve (see inset) gives a mosaic spread for the intense peak as low as 1° at full-width at half-maximum (FWHM) compared to 0.2° for the substrate. According to the $LiFePO_4$ structure [31], this main diffraction peak can be indexed as (0 2 2)/(1 1 2) in the *Pmnb* space group. Besides this intense peak, we can also observe another peak at about $2\theta = 45.1°$ which could be attributed to (1 1 0) reflection of metallic iron. This does not come out of the blue, as we recently reported that metallic iron was formed for samples deposited on (1 0 0) silicon wafers using the same selected set of synthesis parameters [28]. We will come back later on the metallic iron formation.

We will now try to justify the observed preferential orientation taking into consideration both substrate (*Fm*3*m*, $a = 4.213$ Å) and $LiFePO_4$ (*Pmnb*, $a = 6.011$ Å, $b = 10.337$ Å and $c = 4.694$ Å [31])

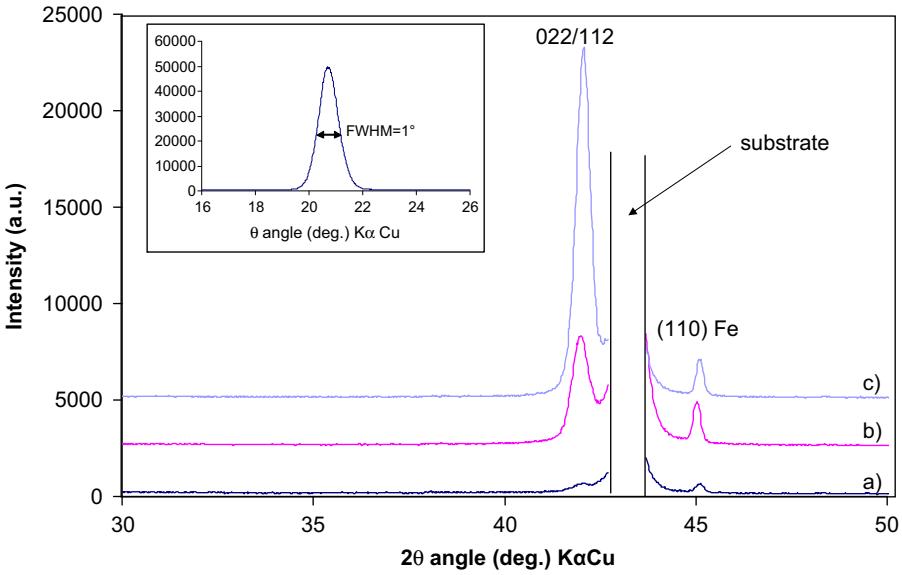


**Fig. 1.** X-Ray diffraction patterns of "$LiFePO_4$" thin films prepared on MgO (1 0 0) substrate under $8 \times 10^{-2}$ mbar Ar at (a) 90 mJ, (b) 150 mJ and (c) 180 mJ laser energy. The insert shows the rocking-curve of the 42.1° intense peak.

unit cells. First, there is no easy lattice match between the main axis of the two structures. If we consider the [1 1 2] orientation for the indexation of the main peak, we did not find any relation between the substrate and $LiFePO_4$ cell parameters. On the other hand, considering the [0 2 2] orientation, we can find a first clue comparing $d(1\,0\,0)_{LiFePO4}$ with $d(1\,1\,0)_{MgO}$ (Fig. 2a). Indeed, the two values (6.011 and 5.958 Å, respectively) differ by less than 1%, meaning that $LiFePO_4$ growth will most likely lead to orientations with $a_{LiFePO4}$ within the substrate basal plane. With this in mind, we evaluated which was the necessary condition for the film to be orientated along the [0 2 2] direction as observed by X-ray diffraction. By geometric considerations (Fig. 2b), we can calculate the interreticular distance $d$ for $LiFePO_4$ along the direction perpendicular to $a_{LiFePO4}$ and parallel to the substrate surface. The relationship between d and the cell parameters is

$$d = \sqrt{\left(\frac{1}{2}b\right)^2 + \left(\frac{1}{2}c\right)^2} = 5.68\,\text{Å}$$

The lattice mismatch between $d(1\,1\,0)_{MgO}$ and $d$ is thus found lower than 5%. We can thus easily understand the observed preferred orientation/texturation along the [0 2 2] direction for the $LiFePO_4$ thin films grown on MgO (1 0 0). For some unknown reasons to now, the growth is not epitaxial as checked by pole figures measurements and only a texturation of the film is observed.

It was then important to further characterize the films in order to get information on their structure and composition not only on the surface but also in the core of the film. For that, we combined electron microscopy (SEM and TEM) with Rutherford backscattering spectroscopy (RBS) measurements. Indeed, we previously reported the importance of microstructure/structure on the electrochemical reactivity of olivine-type thin films [3]. Furthermore, under specific PLD conditions, we recently observed peculiar surface morphologies at the surface of olivine film deposited on (1 0 0) silicon substrate with namely the presence of protuberances, composed partly/fully of metallic iron [28]. Such unusual architecture is still observed in the present films. Fig. 3 shows the surface morphologies observed for samples obtained at different laser energies. As the laser energy increases, the length of the protuberances observed at the surface decrease with a modification of their morphology. Moving to the core film analysis, the simulation performed to fit the RBS spectrum (Fig. 4) indicates that the film composition is very complex. From the variation of Mg, Fe and P species versus thickness, the sample can be decomposed into three different layers denoted MgO, L1 and L2 (Fig. 4). According to these results, during the film growth at 600 °C, there is interdiffusion of iron and magnesium; namely diffusion of iron inside the MgO substrate (corresponding to the L1 region) and diffusion of Mg along the whole PLD-prepared film thickness (corresponding to the L2 region). It is worth noting that the early layers of the

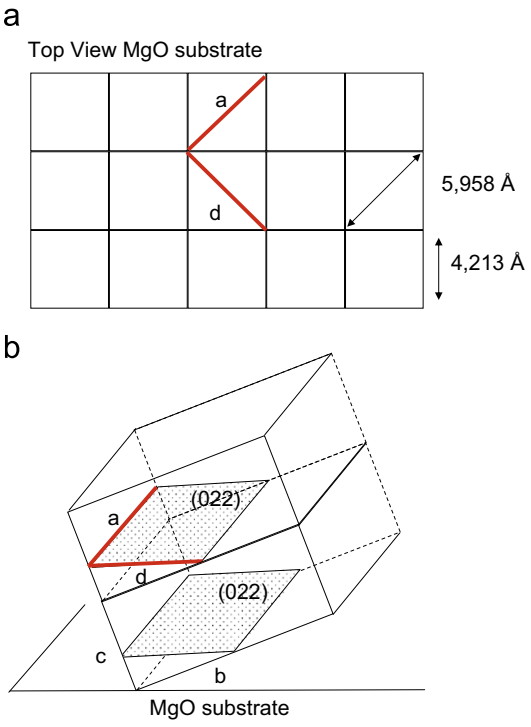


**Fig. 2.** (a) Representation of the possible relationship between the (0 2 2) textured $LiFePO_4$ structure preferentially oriented and the (1 0 0) MgO substrate. (b) In plane relation between LiFePO4 and MgO cells by considering a preferred (0 2 2) orientation of the film.

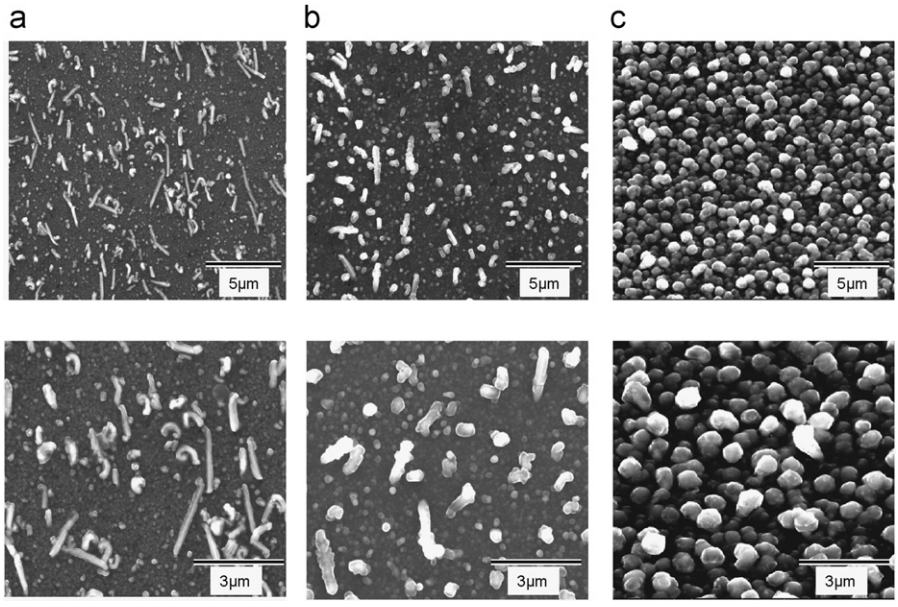


**Fig. 3.** SEM micrograph (obtained at 10 keV and 40° tilt angle) for "$LiFePO_4$" thin films synthesized with different laser energy (a) 90 mJ, (b) 150 mJ and (c) 180 mJ.

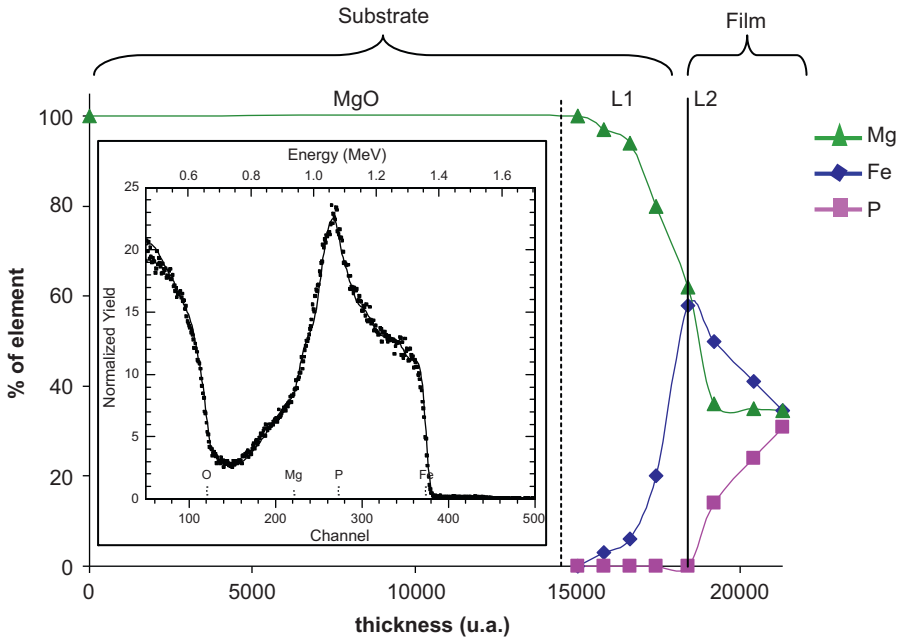


**Fig. 4.** Simulated and experimental RBS spectra for "$LiFePO_4$" thin films grown at a 120 mJ laser energy under $8 \times 10^{-2}$ mbar Ar. The in-depth Mg, Fe and P distributions are also shown.

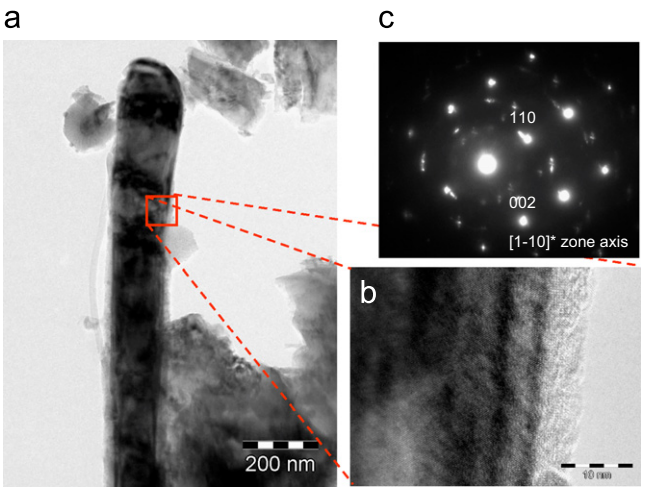


**Fig. 5.** (a) Bright field TEM image of a particle recovered by scratching a film grown at 90 mJ laser energy under $8 \times 10^{-2}$ mbar Ar. (c) High resolution image of the nail head with the HRTEM image and corresponding FFT pattern (b).

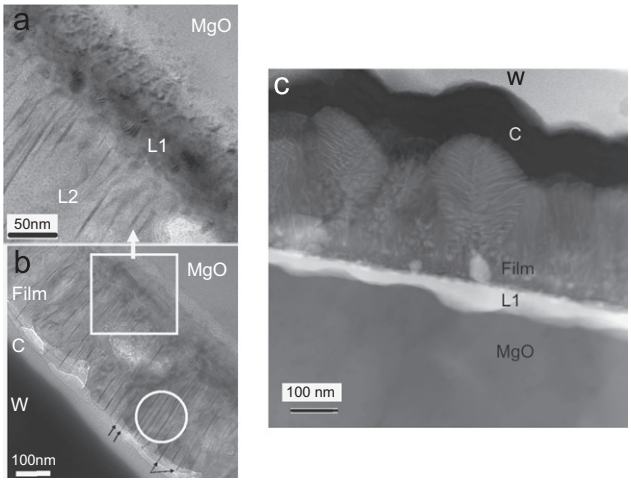


**Fig. 6.** STEM typical images of the FIB-prepared cross section obtained on "$LiFePO_4$" thin films grown at a 120 mJ laser energy under $8 \times 10^{-2}$ mbar Ar. (The (a) image correspond to a closer look of indicated square domain.)

deposited film, close to the substrate, are poor in phosphorous, and the simulation of the RBS spectrum showed a noticeable oxygen deficiency in the overall film, certainly related to the PLD growth under Ar gas.

In order to gain information on the protuberance growth and species diffusion, a thorough TEM study was performed on the sample deposited at 90 mJ laser energy. In a first approach, the films surface was scratched with a stainless steel blade to isolate some protuberances which were deposited on a holey carbon copper grid (in this case the 90 mJ was selected as it presents numerous thin protuberances).

These protuberances (Fig. 5a) are well crystallized as seen by the spot-type selected area electron diffraction (SAED) pattern (Fig. 5c) and the high resolution (HR) image (Fig. 5b) obtained on the edge which shows clearly lattice fringes. The different SAED spots can be indexed using the metallic iron cell parameters and we determinate the zone axis as [1–10]. Such indexation is consistent with the EDS spectrum realized in the nanoprobe mode on the same region showing the solely presence of a peak related to iron.

A focused ion beam cross-section of the thin film was prepared to reveal information on the film core and the interface with the substrate. For such purpose, we examined and compared both the STEM and HAADF images of the FIB cross section (Fig. 6). The different layers evidenced by RBS are nicely observed (Fig. 6a): the MgO substrate, the interface with the film (L1), the film (L2) with the addition of carbon and tungsten layers which were deposited prior to the cross section preparation to protect the surface (Fig. 6c). The images recorded in the bright field mode or HAADF mode reveals an unexpected nanostructuration of the film. It is important to keep in mind that the HAADF contrast is proportional to the atomic number square ($Z^2$) of the elements and thus give some composition information. The interface between the film and substrate does not appear well defined. The L1 layer is about 50 nm thickness (Fig. 6a and c). Beyond this first layer, within the L2 zone, numerous

parallel sharp lines or needles are observed (indicated by arrows in Fig. 6b). For some of them, within grains close to the external surface of the film, the layout of the needles change from parallel to dendritic giving birth to a "leaf veins"-like texture (Fig. 6c). Through a closer look in the HR mode (Fig. 7a) of a typical zone of the film (white circle of Fig. 6b), we distinguish the formation of a nice intergrowth of gray and dark very well-crystallized layers. EDS analysis performed in different zones, for instance Zone 1 in Fig. 7a, allow to attribute a mean composition of 28% Mg, 38% P and 34% Fe for these gray layers. It is worth noting that this result, consistent with RBS analysis reported above, confirms that there is diffusion of magnesium through the entire film. Fast Fourier transform (FFT) calculated from the image at the exact location of Zone 1 can be indexed using olivine cell parameters with [1 0 0] zone axis. On the other hand, EDS quantification from Zone 2 (Fig. 7a) indicates that the darker lines are made of pure iron. Again, the corresponding FFT confirm this, as it can be indexed using metallic iron structure with the $[-1\ -9\ 3]$ zone axis. Drawing of the two implied structures taking into account the structural relationship established from the FFT indexing (Fig. 7b) allows to underline a perfect match along the two determined directions. Indeed, in addition to $[1\,0\,0]_{LFP}//[-1\ -9\ 3]_{Fe}$ and $[0\,2\,1]_{LFP}//[-3\,1\,2]_{Fe}$ topotactic relationships, we can see that a nice interface can be created along the $[01\text{–}1]_{LFP}$ direction where iron atoms line up (dashed line) and could intercalate 5 iron atoms (black arrows) to form one of the compact atomic layer of the metallic iron structure.

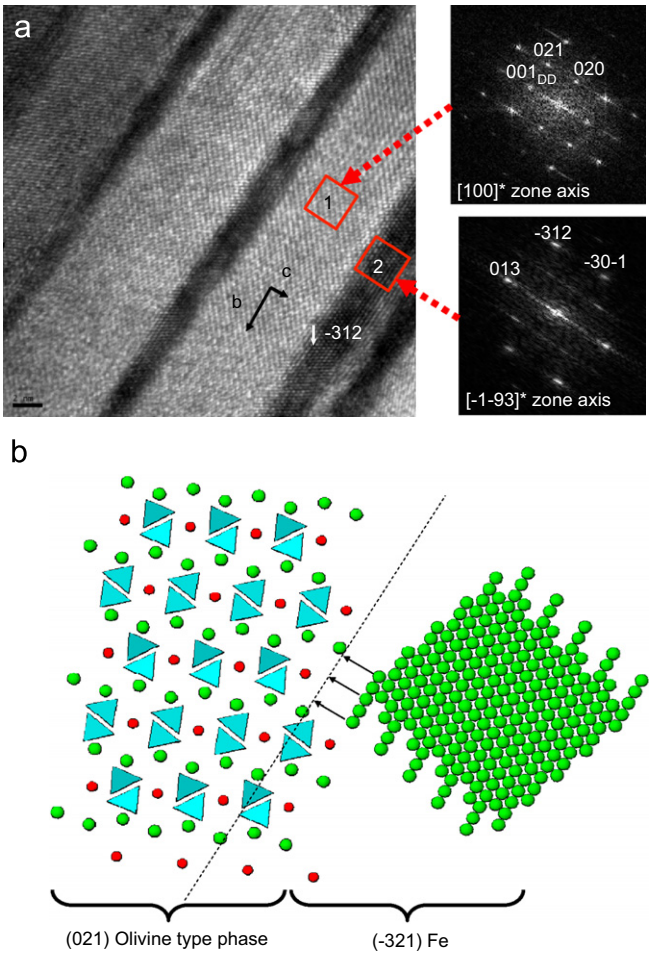


**Fig. 7.** (a) HRTEM image obtained for the FIB cross section obtained on $LiFePO_4$ thin films growth at 120 mJ laser energy. (b) Representation of the possible structural relationship between the olivine and iron metal domains.

Looking back at the film/substrate interface, another HAADF image associated with an EDS line profile analysis was realized (Fig. 8). There is a perfect correlation between the wither region (at the interface) and the increase in iron content. Again, we can conclude that a strong amount of metallic iron is formed at the interface between the substrate and the thin film.

### 3.2. Discussion

The Fe/olivine-type intergrowth within the PLD thin film prepared in this work is amazing. To our knowledge, such an arrangement has never been reported for this kind of materials. On the HRTEM image (Fig. 7), we did not observe any defective zone at the interface between the two phases, consistent with the topotactic relationship demonstrated above. We could wonder however what the origin of such intergrowth is. In order to go towards an answer, we first have to remind that the film was grown at 600 °C. At this temperature, the mobility of iron and magnesium is increased. The crystallization of both oxides, MgO and FeO, within the same rocksalt type structure could lead to the formation of mixed $Mg_{1-x}Fe_xO$ at the interface. However, the large difference between the ionic size of these two ions (0.72 Å for $Mg^{2+}$ and 0.61 Å $Fe^{2+}$ [32]) sweeps away this possibility. Similarly, we could have envisaged the formation of spinel-type $Mg_xFe_yO_4$ previously reported to epitaxially grow on Mg(0 0 1) substrate [33]. However, the formation of a phase comprising $Fe^{3+}$ is not as trivial under the reducing conditions we used. The solely possibility for such formation would be the disproportionation of $Fe^{2+}$ into $Fe^{3+}$ and $Fe^0$ ("$FeO \rightarrow Fe + Fe_2O_3$") which was previously reported either under argon, $H_2$ or CO atmospheres [34]. Such a disproportionation could be induced in our case by the oxygen deficiency which was observed in the films grown under Ar gas. Indeed, it has been recently shown [35] that an oxygen deficiency in indium tin oxide film can induce the formation of a nanocomposite film, i.e. metallic In–Sn clusters embedded in a stoichiometric indium tin oxide matrix. This phase separation is due to the crystallization of the stable stoichiometric indium tin oxide matrix at the expense of the remaining sub-oxide which becomes more and more oxygen deficient, and leads to the metallic cluster synthesis in the extreme limit. A similar explanation could thus be envisaged in our oxygen deficient films.

In the present state it is difficult to definitely conclude about the mechanism for the formation of iron within these films and further investigation are required, notably for the interfacial phase (L1 zone). However, whatever its nature, there should be a structural relationship with the MgO substrate as the olivine phase grow along a specific direction understandable through a MgO/olivine relationship. In this system, two different interfaces thus seem to stabilize the formation of the nanostructure: (1) between the substrate/L1 layer and the olivine phase and (2) between the olivine and metallic iron. Finally, the olivine phase (gray contrast on Fig. 7), is composed of equal quantities of iron and phosphorous together with a high amount of magnesium (about 28%) resulting from solid state diffusion from the substrate. Keeping in mind the closed $Li^+$ and $Mg^{2+}$ ionic radii (0.76 and 0.72 Å, respectively), magnesium ions are expected to occupy the M(1) lithium site leading to a composition $Li_xMg_yFePO_4$ with $x+y<1$ (slight iron deficiency cannot be excluded at the present time).

## 4. Conclusions

Using pulsed laser deposition, we have grown complex thin film nanostructures made of olivine-type phase with preferential orientation (0 2 2) and metallic iron. This latter form layers which crystallize within the olivine structure and form kinds of "columns"

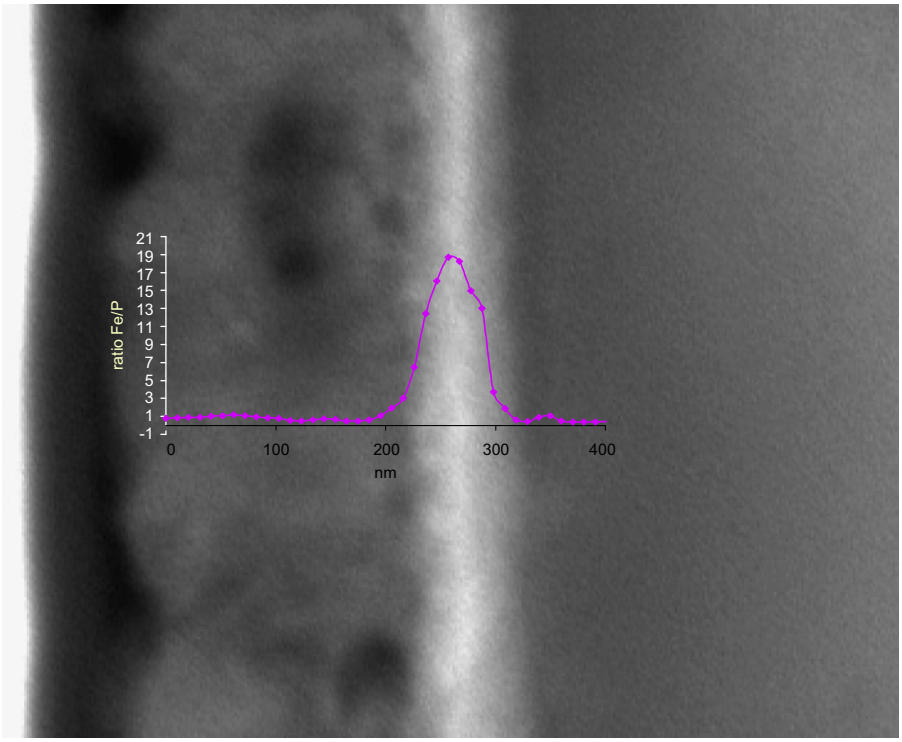


**Fig. 8.** HAADF image and Fe/P ratio calculated from EDS line profile analysis realized at the film/substrate interface of film growth at 120 mJ laser energy.

which give rise to the protuberances visible at the surface of the samples. The perfect overlap between olivine phase and iron cell can be explained by a topotactic relationship. These iron layers are the "germ" of the protuberances growth exclusively composed by iron metal on the samples surface. Furthermore, a diffusion of magnesium from the substrates toward the sample surface involves the formation of an interlayer together with a magnesium-composed olivine phase into which $Mg^{2+}$ ions substitute mainly lithium. All these observations show that at high temperature under low argon pressure a disproportionation of iron(II) occurs. Further studies are now needed to get precise information on the formation mechanism and this could open new interesting studies on a finer control of such nanostructures and the study of their electric of magnetic properties.

## Acknowledgment

Dr. Troadec is acknowledged for his very invaluable participation in the FIB cross-section preparation.

## References

[1] M. Gaberscek, R. Dominko, J. Jamnik, Electrochem. Commun. 9 (12) (2007) 2778.
[2] O. Maqueda, F. Sauvage, L. Laffont, M.L. Martinez-Sarrion, L. Mestres, E. Baudrin, Thin Solid Films 516 (8) (2008) 1651.
[3] F. Sauvage, E. Baudrin, L. Gengembre, J.-M. Tarascon, Solid State Ionics 176 (2005) 1869.
[4] J.W. Lee, S.I. Pyun, Electrochim. Acta 49 (5) (2004) 753.
[5] I. Yamada, T. Abe, Y. Iriyama, Z. Ogumi, Electrochem. Commun. 5 (2003) 502.
[6] M. Hirayama, N. Sonoyama, T. Abe, M. Minoura, M. Ito, D. Mori, A. Yamada, R. Kanno, T. Terashima, M. Takano, K. Tamura, J. Mizuki, J. Power Sources 168 (2007) 493.
[7] A.K. Padhi, K.S. Nanjundaswamy, C. Masquelier, S. Okada, J.B. Goodenough, J. Electrochem. Soc. 144 (1997) 1609.
[8] A. Yamada, S.C. Chung, K. Hinokuma, J. Electrochem. Soc. 148 (3) (2001) A224.
[9] A. Yamada, M. Hosoya, S.-C. Chung, Y. Kudo, K. Hinokuma, K.-Y. Liu, Y. Nishi, J. Power Sources 119 (2003) 232.
[10] P.P. Prosini, M. Carewska, S. Scaccia, P. Wisniewski, M. Pasquali, Electrochim. Acta 48 (2003) 4205.
[11] P.P. Prosini, M. Carewska, S. Scaccia, P. Wisniewski, S. Passerini, M. Pasquali, J. Electrochem. Soc. 149 (2002) 886.
[12] G.X. Wang, S. Bewlay, J. Yao, J.H. Ahn, S.X. Dou, H.K. Liu, Electrochem Solid State Lett. 7 (2004) A506.
[13] K. Rissouli, K. Benkhouja, J.R. Ramos-Barrado, C. Julien, Mater. Sci. Eng. B98 (2003) 185.
[14] C. Delacourt, L. Laffont, R. Bouchet, C. Wurm, J.B. Leriche, M. Morcrette, J.-M. Tarascon, C. Masquelier, J. Electrochem. Soc. 152 (5) (2005) A913.
[15] Y.N. Xu, S.Y. Chung, J.T. Blocking, Y.M. Chiang, W.Y. Ching, Electrochem. Solid State Lett. 7 (2004) A131.
[16] C. Delacourt, P. Poizot, S. Levasseur, C. Masquelier, Electrochem. Solid State Lett. 9 (2006) A352.
[17] N. Ravet, Y. Chouinard, J.F. Magan, S. Besner, M. Gauthier, M. Armand, J. Power Sources 97 (2001) 503.
[18] M. Armand, M. Gauthier, J.-F. Magnan, N. Ravet, WO 02/27823 Patent (2002).
[19] G. Arnold, J. Garche, R. Hemmer, S. Strobele, C. Vogler, M. Wohlfahrt-Mehrens, J. Power Sources 119 (2003) 247.
[20] D. Morgan, A. Van der Ven, G. Ceder, Electrochem. Solid State Lett. 7 (2) (2004) A30.
[21] M.S. Islam, D.J. Driscoll, C.A.J. Fischer, P.R. Slater, Chem. Mater. 17 (2005) 5085.
[22] G. Chen, X. Song, T.J. Richardson, Electrochem. Solid State Lett. 9 (6) (2006) A295.
[23] X.J. Zhu, L.B. Cheng, C.G. Wang, Z.P. Guo, P. Zhang, G.D. Guo, H.K. Liu, J. Phys. Chem. C 113 (32) (2009) 14518.
[24] J. Hong, C.S. Wang, N.J. Dudney, M.J. Lance, J. Electrochem. Soc. 154 (8) (2007) A805.
[25] J. Ma, Q.-Z. Qin, J. Power Sources 148 (2005) 66.
[26] Y. Iriyama, M. Yokoyama, C. Yada, S.K. Jeong, I. Yamada, T. Abe, M. Inaba, Z. Ogumi, Electrochem. Solid State Lett. 7 (10) (2004) A340.
[27] F. Sauvage, E. Baudrin, M. Morcrette, J.-M. Tarascon, Solid-State Lett. 7 (2004) A15.
[28] C. Legrand, L. Dupont, K. Tang, H. Li, X.J. Huang, E. Baudrin, Thin Solid Films 518 (2010) 623.
[29] M. Morcrette, C. Wurm, C. Masquelier, Solid State Sci. 4 (2002) 239.
[30] M. Morcrette, P. Barboux, J. Perrière, T. Brousse, Solid State Ionics 112 (1998) 249.
[31] G. Rousse, J. Rodriguez-Carvajal, S. Patoux, C. Masquelier, Chem. Mater. 15 (2003) 4082.
[32] R.D. Shannon, Acta Crystallogr. A32 (1976) 751.
[33] M.T. Johnson, H. Schmalzried, C.B. Carter, Solid State Ionics 101 (1997) 1327.
[34] W.K. Jozwiak, E. Kaczamarek, T.P. Maniecki, W. Ignaczak, W. Maniukiewicz, Appl.Catal. A: General 326 (2007) 17–27.
[35] M. Nistor, J. Perrière, C. Hebert, W. Seiler, J. Phys.: Condens. Matter 22 (2010) 045006.